

Collisions between rare-gas atoms at low keV energies. I. Symmetric systems

J. C. Brenot, D. Dhuicq, J. P. Gauyacq, J. Pommier, V. Sidis, M. Barat, and E. Pollack*

Laboratoire de Collisions Atomiques, † Bâtiment 220, Université Paris-Sud, 91405 Orsay, France

(Received 1 August 1974)

Elastic and inelastic collisions in the symmetric He-He, Ne-Ne, Ar-Ar, and Kr-Kr systems are investigated experimentally and theoretically at low keV energies (0.5–4 keV). Standard techniques, employing electrostatic energy analysis for ions and time-of-flight methods for neutrals, are used in energy-loss measurements. The characteristic energy spectra of the scattered beams generally show three peaks corresponding to elastic scattering and collisions resulting in one- or two-electron excitations. Of particular significance is the dominance of the lowest-lying p levels in the inelastic scattering. Differential cross sections are determined at select energies and the interpretation of the results is made in the framework of the electron-promotion model. *Ab initio* calculations are performed for the Ne and Ar cases. The primary mechanism in the inelastic scattering always involves one- or two-electron transitions from a promoted incident molecular orbital by rotational coupling for He-He, and by radial coupling in the Ne-Ne and Ar-Ar cases. Predictions based on the assumed model are compared with results of related experiments.

I. INTRODUCTION

It is now well known that inelastic atom-atom scattering may be quite important even at energies as low as several hundred electron volts. The theoretical treatment of such collisional excitation is difficult, and it is desirable to find suitable models that allow the problem to be simplified. Since the appearance of the well-known Fano-Lichten promotion model^{1,2} which explained inner-shell excitations, on a molecular picture, much experimental and theoretical work has been devoted to assess the reliability of this model. In particular there were questions on its applicability to outer-shell problems. A major goal of the present work is a comparison of predictions made on the basis of the promotion model to the observed scattering in neutral symmetric rare-gas systems.

The closed-shell neutral system has received a great deal of attention starting with the pioneering work of Amdur.³ These early experiments on the energy dependence of the total cross section successfully provided much information on the repulsive interatomic potential which was well represented by exponential- and inverse-power expressions. At closer internuclear distances when the shells begin to penetrate, the scattering is no longer purely elastic and such potentials lose their significance.

Scattering studies of alkali ions and neutral rare gases provided the first direct evidence of the importance of inelastic processes in closed-shell systems.^{4–6} In particular experimental results on $\text{Li}^+ + \text{He}$ have shown the importance of one or two $2p$ electron excitation processes. These inelastic processes were explained by a rotational coupling between the incident $2p\sigma$ molecular orbital (MO)

and the excited $2p\pi$ MO. This early work was made possible by electrostatic energy analysis of the scattered charged particles which enabled the participating states to be identified. The same technique has allowed the detailed investigation of ionizing processes in neutral rare-gas collisions.^{7,8} Such studies of ionization in He-He collisions were interpreted in a quasimolecular framework by assuming a primary promotion mechanism which was thought to be common to both ionization and excitation.⁷ The rigorous comparison of theory and experiment, however, required an energy analysis of the scattered neutral projectiles which became possible with the introduction of time-of-flight (TOF) techniques in this energy range.⁹ Although the energy resolution in this early work was relatively poor, the results supported the assumed model. The He-He system is reinvestigated here and the study is extended to include other symmetric rare-gas systems using a TOF apparatus having improved energy resolution.¹⁰ In addition, ionizing collisions are also studied using standard techniques (electrostatic energy analysis) and provide complementary information on the scattering. This method is used in our current studies on He-He and Ne-Ne (the Ar-Ar case has been previously reported⁹). Additional insight into the collision dynamics may, of course, be provided by available photon studies, ejected electron spectra, and total ionization measurements and the results of such studies are incorporated in our discussion.

The current theoretical approach, which has proved successful in dealing with the problem, requires a knowledge of the quasimolecule formed in the collision. Starting with the simplest approach based on a Lichten-type² correlation dia-

studied by the TOF analysis of the incident beam (suitably reduced in intensity): no contribution of excited particles has been found in the spectra showing, in particular, that no substantial amount of metastables is formed in the incident beam. This is in agreement with the previous studies.^{7,9} On the other hand in the case of neon and krypton, the different isotopes have been found; in each case we have chosen the main isotope. In addition the chopping frequency had to be adjusted to allow a complete energy-loss spectrum to lie without any overlap with the corresponding spectra coming from other isotopes. The pressure in the collision chambers is within the region of linear dependence of the count rate versus gas pressure for a given collision process.

Two procedures for taking data have been used. The first one consists of measuring the total number of scattered particles (without chopping) at each scattering angle. This measurement permits the determination of the "summed" differential cross sections for each beam energy. Then the measurement of the relative peak intensity within the spectra, together with the "summed" cross section, yield values for the differential cross section for each process. (We have checked that the measurement of the peak height instead of the area under the peak generally leads to a negligible error.) When the peak is broadened by the presence of several unseparated processes, we have arbitrarily chosen to still use the heights of the peaks. Actually the scattered current is stable enough over a long period of time (3 days minimum with continuous running) to allow a second procedure to be used. This consists of making a direct determination of the cross sections from only the spectra taken at each angle during a preset time (i.e., it is no longer necessary to make a measurement of the "summed" cross section). This is automatically performed using a programmable analyzer (S.E.I.N.) on line in the experiment.

The data are presented as *reduced cross sections*,¹⁵ $\rho \propto I \theta \sin^2 \theta$ (where I is the count rate and θ the laboratory scattering angle) as a function of the reduced angle $\tau = E \theta$ (E is laboratory energy). For angles $\leq 3^\circ$ a suitable apparatus function is used to take into account the limitation of the collision length by size of the collision chamber.

The error on the zero scattering angle is of the order of 0.2 deg. The error in the reproducibility of the data is estimated to be less than 20% (in most cases it is less than 10%). The error introduced in the absolute normalization to the theory (see later) is likely to be no greater than 30%. Estimations of total cross section are given within a factor of 2.

III. He-He COLLISION

The He-He case provides the simplest example of a closed-shell symmetric rare-gas collision system. Only the two electrons in the promoted $2p\sigma_u$ MO are active in the inelastic scattering, while the $1s\sigma_g^2$ core essentially plays no role. This property provided the starting point for the interpretation of ionizing processes occurring in the collision.⁷ The mechanisms proposed involve the promotion of one or two electrons, mainly through $2p\sigma_u-2p\pi_u$ rotational coupling, followed by subsequent couplings with the continua (see Fig. 6 in Ref. 7). The same rotational-coupling mechanism was first introduced to explain inelastic processes involving the excitation of one or two $2p$ electrons in $\text{He}^+ + \text{He}$ collisions.¹³ The model predicts that single-electron promotion should selectively excite the $\text{He}(1s2p)$ state in one of the collision partners, and for the case of two-electron excitation each atom is excited to this state. The ejected-electron spectra¹⁴ provide additional information explainable by the model. Preliminary confirmation of the direct process was provided by TOF measurements.⁹ It was shown that plots of ρ , the reduced cross section,¹⁵ vs τ , the reduced scattering angle, exhibit similar behavior for one- and two-electron excitation when compared to that observed for ionization. Unfortunately these early results were obtained on an apparatus not intended for TOF measurements at relatively high energies and were limited in energy resolution by the short flight path. The present work extends the studies to higher energy (allowing a direct comparison with previous ionization studies) and the resolution is sufficiently good to enable a precise assignment of the participating excited states to be made.

Figure 2 shows typical energy spectra at several incident beam energies and laboratory scattering angles. In Fig. 2(a) three peaks may be seen. The peak labeled *A* corresponds to elastic scattering, peak *B* to one-electron excitation of $\text{He}(1s2p^1P)$ (confirming the dominant excitation resulting from the $2p\sigma_u-2p\pi_u$ coupling), and peak *C* to the simultaneous excitation of both atoms. The smaller two-electron peak shows the excitation of $\text{He}(1s2s^3S)$ which is allowed only in simultaneous excitation (in contrast to the spin-allowed 1P state in the one-electron excitation in peak *B*). Figure 2(b) shows a similar spectrum taken at higher energy (and lower τ). Peak *B* still has its maximum value at the 1P position but displays a tail extending toward higher energy losses demonstrating the participation of higher-lying levels as well as ionization of the target. Peak *C* shows the dominance of the 1P excitation in both partners.

Figure 3 shows the energy spectra of ionized projectiles (obtained on the ion spectrometer) and extends our previous results⁷ to lower energy. Peak B' corresponds to ionization at the threshold energy while C' represents processes involving energy losses greater than 40 eV. At small scattering angles C' is peaked at a 40-eV loss. This ionization is caused by a "Penning"-type process resulting from the excitation of states that at infinite separation lead to $\text{He}(1s2s) + \text{He}(1s2s)$, etc., but which decay during the collision. The simultaneous excitation without Penning ionization is demonstrated in peak C of Fig. 2. A comparison of Fig. 3 with Fig. 2 in Ref. 7 shows the marked energy dependence of the ionizing processes. At higher energy, ionization with simultaneous target excitation is dominant in contrast to the lower-energy case where the simple Penning processes dominate.

The present measurements study the collision over an energy range (E) from 0.35 to 3.0 keV. The data at 0.35 keV are in good agreement with the earlier results.⁹ Figure 4 shows the reduced cross sections (normalized to previous "summed" cross sections obtained from the total number of particles scattered at a given angle) plotted as a function of reduced scattering angle for elastic scattering and scattering with one- and two-electron excitation at incident beam energies of 0.50, 1.00, and 2.00 keV. The elastic cross sections $\rho_{(A)}$ are seen to fall monotonically with a rapid

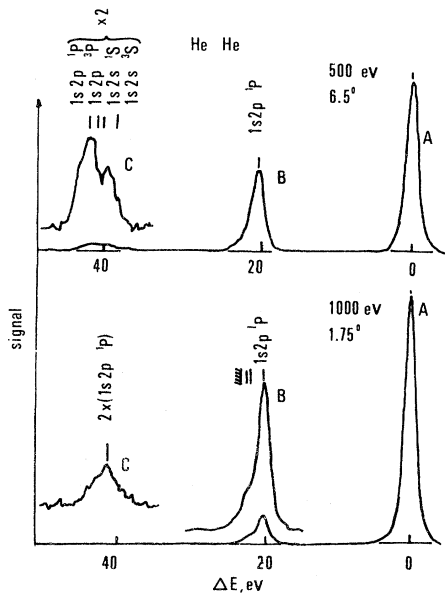


FIG. 2. Energy-loss spectra of scattered He from He-He collisions. The peaks labeled A , B , and C refer to elastic scattering and scattering with one- and two-electron excitations, respectively.

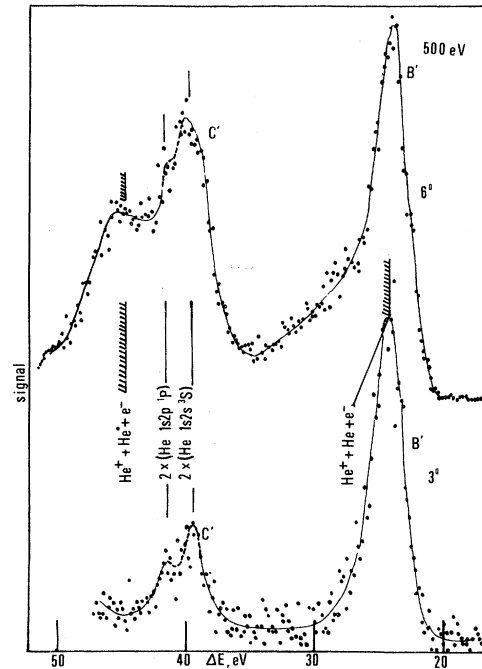


FIG. 3. Energy-loss spectra of scattered He^+ from ionizing He-He collisions. The underlying line is an estimate of the spectrum drawn through the data points.

decrease at $\tau = 3$ keV deg due to the opening of inelastic channels. Of particular significance is the shift of the maxima of the one- (ρ_B) and two-electron (ρ_C) excitation cross sections toward lower reduced scattering angles with increasing

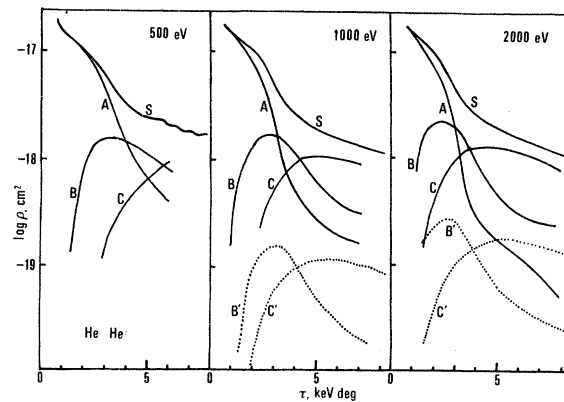


FIG. 4. Reduced differential cross sections for He-He collisions as a function of reduced scattering angle. The curves labeled A , B , and C refer to elastic scattering and scattering with one- and two-electron excitation, respectively. Curves B' and C' represent simple ionization and ionization with target excitation, respectively, while curve S represents the sum over the elastic and all the inelastic (including ionization) cross sections. The S , B' , and C' curves are taken from Ref. 7.

beam energy. In the one-electron excitation case this maximum is found to shift from its position at $\tau=3.7$ keV deg at 0.35 keV down to $\tau=2.4$ keV deg at 2.0 keV. This behavior (including the absence of oscillations) is characteristic of a rotational coupling¹⁶ occurring near the united-atom limit. Similarly, for the two-electron excitation the maximum in the reduced cross section shifts from a reduced scattering angle greater than 8.0 keV-deg at 0.25-keV beam energy to about 4.5 keV deg at 2.0 keV. The two lower curves ρ'_B and ρ'_C represent simple ionization and ionization with target excitation. It is quite striking that these curves behave very much like the one- and two-electron excitation curves, respectively. This was expected on the basis of the proposed model⁷ which attributes both excitation and ionization to the same primary mechanism ($2p\sigma_u-2p\pi_u$ rotational coupling). A second interesting feature is displayed by the common values of the $\rho_B-\rho_C$ and $\rho'_B-\rho'_C$ crossing-point position as well as by the equal ratios $2\rho'_B/\rho_B$ and $2\rho'_C/\rho_C$; the factor 2 accounts for target ionization which is included neither in ρ'_B nor in ρ'_C , whereas the neutral curves ρ_B and ρ_C represent both target and projectile excitation. For instance, at beam energies of 1 and 2 keV, this common ratio amounts to 0.18 and 0.25, respectively. These features imply that the same mechanism is involved in coupling with the continuum in both cases. These ratios should provide useful information to further check theoretical calculations on heavy-particle collisional ionization.

IV. Ne-Ne, Ar-Ar, AND Kr-Kr COLLISIONS

Although the heavier symmetric systems are potentially more complex than the He-He case, generally only two electrons are actively involved in inelastic processes at low keV energies. These active electrons belong to the strongly promoted outermost σ_u MO ($4f\sigma_u$ for Ne-Ne, $5f\sigma_u$ for Ar-Ar, and $6f\sigma_u$ for Kr-Kr). In terms of the simple Fano-Lichten model the crossing of this promoted MO with empty excited MO's can result in one- or two-electron promotion, thereby giving rise to three peaks in the energy-loss spectra at τ values corresponding to the crossing region. This may indeed be seen in Fig. 5 for the Ar-Ar ($\tau=5.5$ keV deg) case. Also shown in the figure are the relative probabilities for producing zero- (A), one- (B), or two-electron (C) excitations in this "triple-peak region." A striking feature of the characteristics associated with zero-, one-, or two-electron transitions from a promoted orbital may be seen when we compare the effect of the outer $5f\sigma_u$ MO promotion with the $4f\sigma_u$ inner-shell¹⁸ promo-

tion. Figure 5(c) demonstrates this and shows the basic similarities for outer and inner MO processes in these systems. It is significant that a similar triple-peak behavior was observed for the related ion-atom system^{19,20} $\text{Ar}^+ + \text{Ar}$ and also in $\text{Ne}^+ + \text{Ne}$.^{19,20} To a first approximation, inelastic processes are seen to proceed via the same basic mechanism in the atom-atom and ion-atom cases.

The Ne-Ne and Ar-Ar cases are presented in the greatest detail starting from *ab initio* calculations, while similarities in Kr-Kr are discussed qualitatively. The theoretical calculations for several possible excitation mechanisms are discussed and compared with our experimental results as well as with those obtained from ion spectroscopy, electron spectroscopy, and optical studies. As will be seen, the problem is still

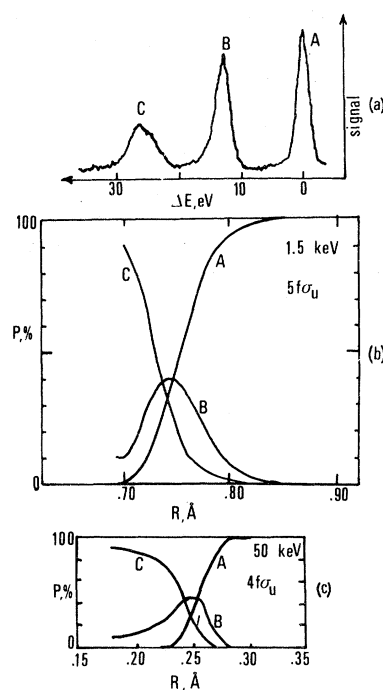


FIG. 5. Characteristics of the scattering associated with a strongly promoted σ MO (a) A typical energy-loss spectrum showing the triple-peak region in Ar-Ar at a 1.5-keV beam energy. The peaks labeled A, B, and C represent elastic scattering, and scattering with one- and two-electron excitations, respectively. (b) The probability of zero- (A), one- (B), or two-electron (C) excitation from the promoted $5f\sigma_u$ MO as a function of the distance of closest approach (obtained from a screened Coulomb potential from Ref. 17) in the Ar-Ar collision. The probabilities are obtained as the ratio of each peak height (A, B, C) to their sum. (c) Electron excitation arising from the promoted inner $4f\sigma_u$ MO in $\text{Ar}^+ - \text{Ar}$ collisions (taken from Ref. 18). The notation is the same as in (b). A comparison between (b) and (c) demonstrates the basic similarities for the outer and inner MO processes in closed shells.

open and requires further experimental and theoretical consideration.

A. Ne-Ne collisions

1. Spectra

The Ne-Ne collision is studied in the energy range from 0.75 to 3.0 keV. Typical neutral spectra are shown in Fig. 6. The lowest-lying inelastic peak (*B*) is dominated by the excitation of the Ne($2p^53p$) level over a large range of τ values. At small values of τ (less than 4 keV deg) there is some evidence for the excitation of Ne($2p^53s$). The asymmetric broadening of the peak toward higher-energy loss is already present at somewhat larger values of τ [see Fig. 6(a)] showing that other one-electron processes are weakly but simultaneously excited. Two-electron excitation processes are likewise dominated by the symmetric $2\text{Ne}(2p^53p)$ excitation. This peak shows a marked broadening toward higher energy loss as the scattering angle increases. Energy losses as large as 60 or 70 eV are found for $\tau > 12$ keV deg where the two-electron processes are in fact the only important ones. Spectra resulting from ionizing collisions may be seen in Fig. 7 and have roughly the same behavior as the neutral spectra.

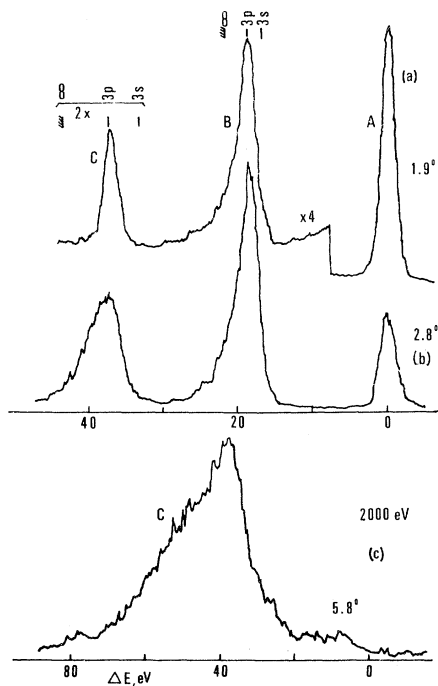


FIG. 6. Energy-loss spectra of scattered Ne from Ne-Ne collisions. The same notation is used as in Fig. 1. (a) and (b) show the dominance of the Ne($2p^53p$) excitation. (c) shows the importance and marked broadening of the two-electron excitation peak at the larger scattering angles.

The simple ionization process, however, initially peaked at the energy threshold, displays a shift in its position which oscillates with τ (this point will be discussed later). Ionization processes accompanied by excitation (peak *C'*) are seen to give rise to broad peaks at large τ values. This broadening is similar to that observed in the neutral spectra (peak *C*) since basically the same processes are involved.

2. Cross sections

Reduced cross sections, corresponding to several processes in Ne-Ne collisions, are presented as a function of τ , the reduced scattering angle, in Fig. 8. The same notations are used as in Fig. 4. At small values of τ the elastic cross section (ρ_A) is normalized to the purely classical elastic cross section obtained using the diabatic incident potential which will be discussed in the theoretical subsection which follows. It may be seen that the typical "triple-peak" behavior occurs for τ values of about 6 keV deg (the analogous behavior occurs at about 9 keV deg in^{19,20} Ne⁺-Ne). The inelastic cross sections display an oscillatory structure which is particularly marked in ρ_B and ρ_B' . This structure has the same phase in the two curves and is characteristic of a Stueckelberg oscillation since the period is found to be proportional to $E^{1/2}$. The slight shift in the location of the first maxima in ρ_B and ρ_B' should be noted. It can also be seen that the ρ_C and ρ_C' curves basically exhibit a similar behavior. Reduced cross sections for ionization (ρ_B' and ρ_C') are plotted, for several Q (inelastic energy loss) values, in Fig. 9. It may be

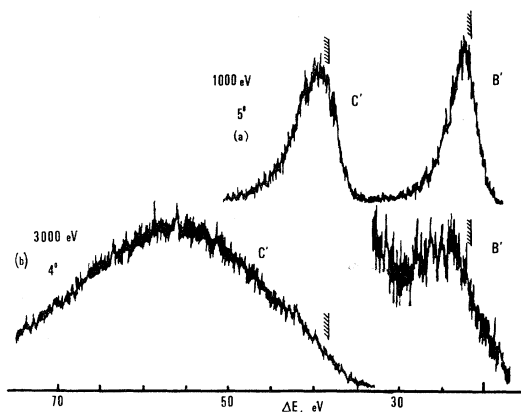


FIG. 7. Energy-loss spectra of scattered Ne⁺ from ionizing Ne-Ne collisions. (a) The ionization peaks *B'* and *C'* have their maxima at threshold and both peaks are narrow. (b) The spectra in these harder collisions [compared to (a)] show the dominance and considerable broadening of *C'*.

seen [Fig. 9(a)] that the curves are shifted towards larger τ values as Q increases. This shift coupled with the oscillatory behavior of the curves is of course reflected in the shifted maximum of the B' peak in the ion spectra (Fig. 7). Similar behavior is observed for C' processes.

3. Qualitative predictions: Diabatic correlation diagram

The Ne-Ne system prior to collision is described by a $1s^2 2s^2 2p^6$ configuration in each atom. As the collision progresses, the molecular character evolves and may be represented by the diabatic electron correlation diagram for Ne_2 as shown in Fig. 10. Details about its calculations are given in Sec. IV A. The incident ground-state MO configuration of Ne_2 is $1s\sigma_g^2 2p\sigma_u^2 2s\sigma_g^2 3p\sigma_u^2 3d\sigma_g^2 2p\pi_u^4 3d\pi_g^4 4f\sigma_u^2$ and corresponds to a molecular state which is repulsive at small internuclear separation. As Fig. 10 shows, the $4f\sigma$ electrons are promoted at the largest internuclear separation, and as a result they are expected to be important in small-angle inelastic scattering. In the simplest model it is convenient to consider two possible sets of crossings.

(a) First, σ MO's correlating to Ne(3s): The first crossing occurs with the $3s\sigma_g$ orbital and, since the u or g character of the entire molecular wave function cannot change, only two electron trans-

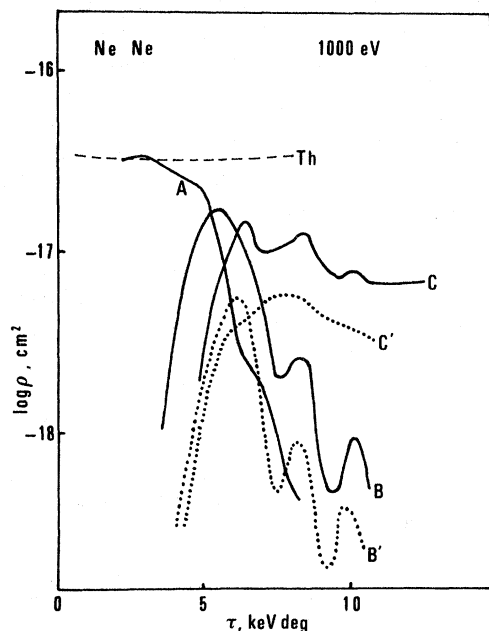


FIG. 8. Reduced differential cross sections for Ne-Ne collisions as a function of reduced scattering angle. The same notation is used as in Fig. 3. The curve labeled Th represents the calculated elastic cross section (see text) used for calibration.

sitions are allowed. One- and two-electron excitation is, of course, possible at the $4p\sigma_u$ crossing. Since the crossing between these orbitals may excite one or two electrons from $2p$ to $3s$ levels in either one or both of the collision partners, the prominence of $3p$ excitation in the experimental results is not easily explained by these MO crossings.

(b) Second, σ and π MO's correlating to Ne($3p$): The σ MO's correlating to the Ne($3p$) level are expected to participate only in hard collisions

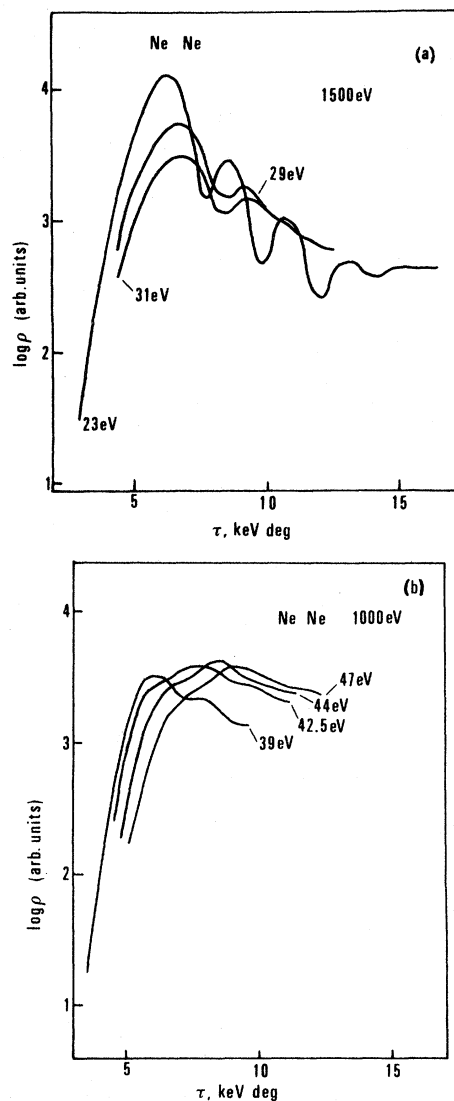


FIG. 9. (a) Differential cross sections for simple ionization (B' peak) in Ne-Ne at several energy-loss values. Note the phase shifts between the curves. (b) Differential cross sections for ionization with simultaneous excitation (C' peak) in Ne-Ne at several energies. Note the shift of the maxima toward higher τ values as the energy-loss increases.

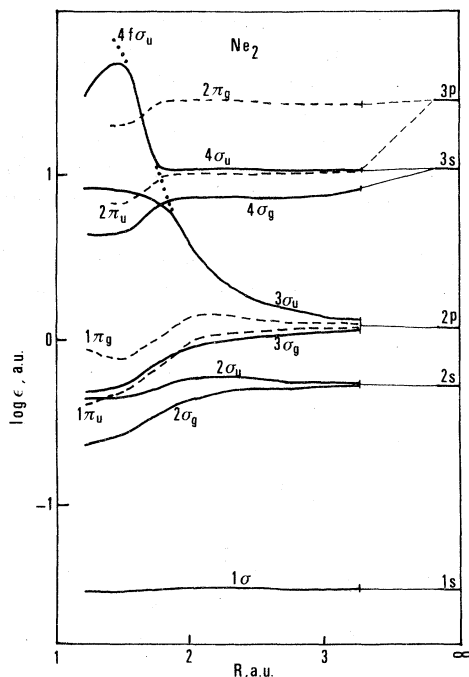


FIG. 10. Calculated adiabatic MO correlation diagram for Ne_2 . Of particular significance is the $3\sigma_u$ - $4\sigma_u$ avoided MO crossing and the estimated $4f\sigma_u$ diabatic promoted MO (shown by the dotted curve).

(since they lie above those correlating to the $3s$ level) and are not discussed. On the other hand, the π_u MO arising from $\text{Ne}(3p)$ can rotationally couple to the $4f\sigma_u$ MO giving rise to selective excitation of one or two $3p$ electrons in moderate collisions, as has indeed been seen in the experimental results. This mechanism is similar to the one discussed in the He-He case except for the location of the crossing point which in Ne-Ne occurs at finite internuclear separation instead of at the united-atom limit. At a first glance the generalization of the rotational coupling to this heavier system appears straightforward, but as

$$\left. \begin{array}{l} C \quad 3\sigma_g^2 4\sigma_g^2 \\ D \quad 3\sigma_g^2 4\sigma_u^2 \\ E, F \quad 3\sigma_g 3\sigma_u 4\sigma_g 4\sigma_u \\ G \quad 3\sigma_u^2 4\sigma_g^2 \\ H \quad 3\sigma_u^2 4\sigma_u^2 \end{array} \right\} \left\{ \begin{array}{l} C', D' \quad \text{Ne}(2p^5 3s) + \text{Ne}(2p^5 3s) \\ E' \quad \text{Ne}^-(2p^5 3s^2) + \text{Ne}^+(2p^5) \\ F' \quad \text{Ne}(2p^6) + \text{Ne}(2p^4 3s^2) \\ G' \quad \text{Ne}^-(2p^5 3s) + \text{Ne}^+(2p^4 3s) \\ H' \quad \text{Ne}^-(2p^6 3s^2) + \text{Ne}^+(2p^4) \end{array} \right.$$

In the absence of u - g symmetries, only a single molecular state is required for two-electron excitation. The proper linear combination of molecular states leading to each of the listed separated atom states is determined by diagonalizing

will be seen a more detailed investigation demonstrates that the problem is not so simple and requires a detailed examination of the molecular states.

4. Choice of the molecular states to be calculated

In practice the required molecular calculations are performed on a quasidiabatic basis set²¹ represented by single configuration of adiabatic MO's. In this representation the incident state is written $(1\sigma_g^2 1\sigma_u^2 2\sigma_g^2 2\sigma_u^2 1\pi_u^4 1\pi_g^4) 3\sigma_u^2 3\sigma_g^2$.

Since the first six orbitals are not involved in the scattering considered here and do not change, the discussion below is concerned only with this "core" and with the four $3\sigma_u^2 3\sigma_g^2$ outer electrons. As the collision evolves, the $4f\sigma_u$ orbital changes character starting as $3\sigma_u$ at large separation and evolving (as may be seen in Fig. 10) through a $3\sigma_u$ - $4\sigma_u$ mixture, to $4\sigma_u$, then through a $4\sigma_u$ - $5\sigma_u$ mixture to $5\sigma_u$.

In order to discuss excitation mechanisms (involving radial couplings) the $4f\sigma_u$ - $3s\sigma_g$ and $4f\sigma_u$ - $4p\sigma_u$ crossings are investigated theoretically in terms of the crossing of the $3\sigma_u$ - $4\sigma_g$ MO's and the pseudocrossing of the $3\sigma_u$ - $4\sigma_u$ MO's. These two interactions cause the excitation of both one and two electrons to $3s$ levels. As the incident channel is $^1\Sigma_g^+$, we consider therefore only states of the same symmetry which result from the excitation of one or two electrons from 3σ to 4σ orbitals. Because of the u - g symmetries in Ne_2 , one-electron excitation results in the configurations (core) $3\sigma_g^2 3\sigma_u 4\sigma_u(A)$ and (core) $3\sigma_u^2 3\sigma_g 4\sigma_g(B)$. The separate single $3s$ excited atomic states are $\text{Ne}(2p^6) + \text{Ne}(2p^5 3s)(A')$ and $\text{Ne}^+(2p^6) + \text{Ne}^-(2p^6 3s)(B')$. States (A') and (B') are each expressible as linear combinations of the molecular (A) and (B) states. For two-electron excitation the u - g symmetries result in six different molecular configurations which when properly combined describe the correct atomic behavior at infinite separation:

the Hamiltonian matrix in the above sixfold subspace. Each of the subspaces corresponding to single and double excitation is constructed from configurations differing by at least two spin orbitals. In the basis set C, D, E, F, G, H the d/dR

matrix elements are zero as is also the case for $\langle A|(d/dR)|B\rangle$. In each subspace the configurations are therefore diabatic in the sense defined by Smith.¹¹

In the case of Ne_2^+ , only the $3\sigma_g^2 3\sigma_u^2 \Sigma_u^+$ and $3\sigma_u^2 3\sigma_g^2 \Sigma_g^+$ levels of the four possible "ground states" are considered. To study ionization with simultaneous excitation of the partner the following states are also considered:

$$\left. \begin{array}{l} J \quad 3\sigma_g^2 4\sigma_g \\ K \quad 3\sigma_u^2 4\sigma_g \\ L, M \quad 3\sigma_g 3\sigma_u 4\sigma_u \end{array} \right\} \left\{ \begin{array}{l} \text{Ne}(2p^5 3s) + \text{Ne}^+(2p^5) \\ \text{Ne}(2p^6) + \text{Ne}^+(2p^4 3s) \\ \text{Ne}^-(2p^6 3s) + \text{Ne}^{2+}(2p^4) \end{array} \right.$$

As in the neutral case discussed above, four molecular configurations are needed to properly describe the separated particle behavior. The four configurations are also diabatic in this subspace.

In order to study the rotational coupling, we have investigated the states representing the excitation of one or two electrons from the $3\sigma_u$ to the $2\pi_u$ orbital. Single excitation provides two different configurations (core) $3\sigma_g^2 3\sigma_u 2\pi_u(A)$ and (core) $3\sigma_u^2 3\sigma_g 2\pi_g(B)$ resulting in the $\text{Ne}(2p^5 3p) + \text{Ne}(2p^6)$ and $\text{Ne}^+(2p^5) + \text{Ne}^-(2p^6 3p)$ separated atomic states. For double excitation only the ${}^1\Sigma_g^+$ and ${}^1\Delta_g$ states must be considered here. In these cases we study the six molecular configurations and six separated atom states below:

$$\left. \begin{array}{l} 3\sigma_g^2 2\pi_u^2 \\ 3\sigma_g^2 2\pi_g^2 \\ 3\sigma_u^2 2\pi_u^2 \\ 3\sigma_u^2 2\pi_g^2 \\ 3\sigma_g 3\sigma_u 2\pi_u 2\pi_g \end{array} \right\} \left\{ \begin{array}{l} \text{Ne}(2p^5 3p) + \text{Ne}(2p^5 3p) \\ \text{Ne}^-(2p^5 3p^2) + \text{Ne}^+(2p^5) \\ \text{Ne}(2p^6) + \text{Ne}(2p^4 3p^2) \\ \text{Ne}^-(2p^6 3p) + \text{Ne}^+(2p^4 3p) \\ \text{Ne}^{2-}(2p^6 3p^2) + \text{Ne}^{2+}(2p^4) \end{array} \right.$$

TABLE I. Slater-type orbitals used in the molecular calculation on Ne_2 .

nl	ζ
1s	14.319
1s	9.224
2s	2.518
3s	5.619
3s	1.4569 ^a
3s	0.837 ^a
2p	6.620
2p	3.484
2p	2.766
3p	1.075 ^a
4p	0.750 ^a
3d	2.200

^a These terms have been added to the basis set of Ref. 24 to allow a correct description of excited states.

5. Molecular *ab initio* calculations

Calculations of potentials are made over the range of internuclear separation from 1.2 to 20 bohr.²² The adiabatic orbitals and the resulting energies of the molecular states are determined from linear combination of atomic orbitals Slater-type orbitals (LCAO-STO) molecular-orbital self-consistent-field (MO-SCF) approximations¹² carried out by the ALCHEMY program of Bagus *et al.*²³ Table I lists the values of the ζ coefficients for the STO's of our basis set. Such a basis set with a few STO's describing one atomic orbital allows for flexibility and balances the nonvariation of the ζ coefficients as a function of R . For internuclear distances less than 1.5 bohr, the u basis orbitals become linearly dependent requiring the deletion of one of them ($3s - \zeta = 0.837$) in order to avoid convergence problems. The SCF variational procedure has been carried out on only the $X^1\Sigma_g^+$ and $C^1\Sigma_g^+$ states of Ne_2 and $X^2\Sigma_u^+$ and $J^2\Sigma_g^+$ states of Ne_2^+ ; the other states have been obtained in the virtual-orbital approximation¹² using the $\text{Ne}_2^+ X^2\Sigma_u^+$ ground state. When the two computational methods were possible, the inaccuracy of the virtual-orbital approximation could be estimated to at most 2 eV. This precision is thought to be sufficient in a study of atomic collisions in the keV energy range. Our STO basis set being very close to that of Gilbert and Wahl,²⁴ leads to results on the $\text{Ne}_2 X^1\Sigma_g^+$ state which are in good agreement with theirs. For the Ne_2^+ ground states, our results were found to be slightly lower than those of Thulstrup and Johansen.²⁵ To our knowledge we report the first calculations on excited states of Ne_2 .

From the $X^1\Sigma_g^+$ and $D^1\Sigma_g^+$ potentials (derived from adiabatic MO's) we have estimated the diabatic potentials by using an interpolating fit

TABLE II. A comparison between some "ground-state" potentials for Ne_2 : (a) The present SCF results and (b) the present incident diabatic potential. GW are the results of Gilbert and Wahl (Ref. 24) and GN are the results of Gaydaenko and Nikulin (Ref. 32). S are the results of Smith (Ref. 32) and GK the results of Gordon and Kim (Ref. 32). Atomic units [R (bohrs), $V(R)$ (hartrees)] are used.

R	(a)	(b)	GW	GN	S	GK
1.4	3.303	3.751	...	3.901	4.752	...
1.5	2.766	2.940	...	3.091	3.732	2.907
1.8	1.724	1.724	...	1.537	1.808	...
2.0	1.105	1.105	...	0.965	1.115	0.9436
2.5	0.326	0.326	0.330	0.302	0.333	0.2985
3.0	0.096	0.096	0.0976	0.094	0.01	0.0901
4.0	0.008	0.008	0.0085	0.0092	0.0089	0.0066

around the pseudocrossing lying at about 1.6 bohr. The incident diabatic potential is compared with previous calculations in Table II. Results showing the potentials for the ground state and for some excited and ionic states are presented in Fig. 11. Byproducts of these calculations are the orbital energies defined as the eigenvalues of the Fock operators.¹² These orbital energies lead to the correlation diagram presented in Fig. 10. This diagram is in agreement with the one previously proposed by Thulstrup and Johansen.²⁵ In addition it shows the $4\sigma_u$ orbital and its pseudocrossing with the $3\sigma_u$ one; this allows the estimation of the promotion of the diabatic $4f\sigma_u$ MO.

6. Discussion

It should be emphasized at this point that it is the molecular states and their related crossings that must be considered in analyzing the collision problem. Although the first MO crossing occurs between the $4f\sigma_u$ and $3s\sigma_g$ orbitals, calculations of the potential curves show that the first potential curve crossing (for g symmetry) involves the $A\Pi_g$ state arising from the one-electron transition $3\sigma_u$ to $2\pi_u$ ($4f\sigma_u$ to $3p\pi_u$). The position of this first crossing implies that a rotational coupling mechanism should be responsible for inelastic scattering involving one-electron excitation at small τ . In particular the selective excitation of $\text{Ne}(3p)$ would be understandable. In order to study this process we evaluate the necessary matrix elements, $(v_0 b/R^2) \langle 2\pi_u | L_y | 3\sigma_u \rangle$ (where v_0 is the incident-beam velocity, b the impact parameter, R the internuclear separation, and L_y the component of the total electronic orbital angular-mo-

mentum operator perpendicular to the collision plane), at values of R where the wave functions are known. At a beam energy of 1.0 keV an interaction of 0.07 eV is obtained at the crossing position ($R_x = 1.9$ bohr, $b = 1.5$ bohr). This interaction is thought to be too small to account for the observed strong inelastic processes. An estimation using the Landau-Zener-Stueckelberg (LZS) model leads to a cross section for this process which is two orders of magnitude too small to account for the experimental value. In addition, the energy value at the X - A crossing point (37 eV) cannot account for the energy threshold behavior observed for several measured total cross sections (see later discussion). The location of the angular threshold for one-electron excitation processes (experimental—5.5 keV deg; theoretical—4.5 keV deg) is also in poor agreement.

The next potential crossing is related to the first σ - σ MO crossing, $4f\sigma_u$ - $3s\sigma_g$ ($3\sigma_u$ - $4\sigma_g$), and gives rise by two-electron transitions not only to $3\sigma_u^2$ - $4\sigma_g^2$ processes but also to an infinite series (labeled C) of quasidiabatic crossings between the incident channel and the Rydberg series $4\sigma_g n\sigma_g$ ($n \geq 4$). These crossings lie in the range $1.6 < R < 1.8$ bohr with the lower value of R corresponding to the crossing with the continuum associated with the $3\sigma_g^2 4\sigma_g$ ionic configuration.

The next MO pseudocrossing ($3\sigma_u$ - $4\sigma_u$) leads to an infinite series of crossings involving the Rydberg states $3\sigma_g^2 3\sigma_u n\sigma_u$ (A series— $n \geq 4$) and $3\sigma_g^2 4\sigma_u^2$ since now both one- and two-electron transitions are allowed. Crossings with an infinite series of continua ending in $\text{Ne}_2^{++} 3\sigma_g^2$ must also be considered at small internuclear separation.

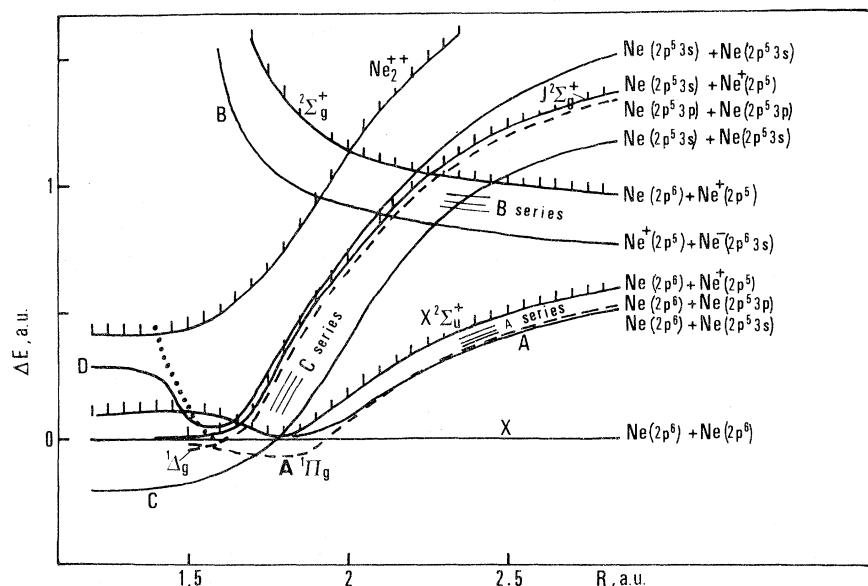


FIG. 11. Several potential-energy curves for Ne_2 and Ne_2^+ referred to the $X^1\Sigma_g^+ 3\sigma_g^2 3\sigma_u^2$ level. The estimated incident diabatic channel corresponding to the $4f\sigma_u$ promotion is represented by the dotted curve.

Two-electron processes involving the $2\pi_u$ MO generate two series of potential curves of ${}^1\Sigma_g^+$ and ${}^1\Delta_g$ symmetries. Excitation of the ${}^1\Delta_g$ states involves two rotational coupling steps and may account for selective excitation of $2\text{Ne}(2p^53p)$. All the possible transitions make the problem complex and only the first X - C crossing is considered in any detail below. Before this is done, however, one additional point should be mentioned. As may be seen from the molecular-potential diagram in Fig. 11, a pinching between the incident $X^1\Sigma_g^+$ channel and the ground state $X^2\Sigma_u^+$ of Ne_2^+ occurs at 1.8 bohr. This region is well localized and the infinite A series [(core) $3\sigma_g^2 3\sigma_u n\sigma_u$] of singly excited molecular states passing through is compressed in it and provides the possibility for direct transitions leading to singly excited final states. These transitions are thought to be weak since couplings through the electronic Hamiltonian between the ground and singly excited states vanish in the virtual-orbitals approximation.²⁶ In addition, the dynamical coupling [$v_R \langle X^1\Sigma_g^+ | (d/dR) | A^1\Sigma_g^+ \rangle$, where v_R is the radial velocity] is estimated to have a value of about 0.1 eV, at the location of the X - C crossing point, for a radial velocity (at the crossing point) resulting in a reduced scattering angle of 6 keV deg. Thus direct transitions between X and A in this region are thought to have little effect on the X - C mechanism. This assumption will be confirmed by its consequences.

The quasidiabatic X - C crossing will be shown to be the important one in accounting for the observed small-angle inelastic scattering. This crossing is well described in a quasidiabatic basis²² and all its characteristics are obtained from *ab initio* calculations ($R=1.784$ bohr, $V=1.772$ hartree = 48 eV, $H_{X-C}=0.44$ eV). Following the primary excitation (X - C) subsequent couplings of C with curves of the A series feed all the singly excited states and the first ionization continuum. On its way out the C state crosses the B series of configuration $3\sigma_u^2 3\sigma_g n\sigma_g$ and fortunately couples with only the lowest-lying B curve ($3\sigma_u^2 3\sigma_g 4\sigma_g$), the others differing from C by three MO's. At larger internuclear distances (4 bohr) the first B state and the A states mix and resolve to the $\text{Ne}^-(2p^63s) + \text{Ne}^+(2p^5)$ and $\text{Ne}(2p^53s) + \text{Ne}(2p^6)$ states. These channels are strongly coupled in the adiabatic basis. In an ionization measurement it is, of course, impossible to determine whether the detected Ne^+ results from the B states or from a direct interaction between the C state and a low-lying continuum state. The calculations made here are only for the latter process. The C state at large internuclear separation mixes by configuration interaction with the five other doubly excited states and as has been shown by computing the dy-

namical coupling (due to d/dR) in the adiabatic basis, uniquely leads to symmetrical excitation of $2\text{Ne}(2p^53s)$. In summary, we consider only those interactions arising from the primary X - C coupling followed by subsequent interactions of C with the A series and B state to explain single excitations, ionization, and symmetrical $3s$ excitation (at least near threshold). Since the primary mechanism is unique to all the studied channels and further interactions (leading to $3s$, $3p$, etc.) are responsible principally for branching ratios, the oscillations seen in the experimental reduced cross sections should reflect the phase interference introduced by this primary X - C crossing. Theoretical reduced cross sections are calculated in the semiclassical approximation using the LZS model. These reduced cross sections are found by using the common incident X channel, common potentials inside the crossing, followed by exit potentials appropriate for each process. In studying a particular reaction it is assumed that only that single channel is populated. Figure 12 shows a comparison of the experimental and theoretical reduced-cross-section results at 1.0 keV for single excitation and at 2.0 keV for simple ionization with zero energy emitted electrons. The position of the first maximum and the oscillatory structure are seen to be in good agreement. A valid comparison of the absolute reduced cross sections is possible only at the first maximum which is relatively free of absorption effects²⁷ occurring at larger τ values and due to the opening of a large number of inelastic channels. The use of a single exit state in the calculation allows a comparison of only the absolute value of the theoretical reduced cross sections with the sum of the single-electron excitation reduced cross section and the simple ionization reduced cross sections (which is here two times the experimentally observed value). Reasonably good agreement between theory and experiment (at the first maximum) is found with reduced cross sections values of 1.45×10^{-17} cm²/sr and 2.6×10^{-17} cm²/sr, respectively (at 1.0 keV as an example). We can therefore conclude that both single-electron excitation ($3s$, $3p$, $4s$, etc.) and simple ionization are reasonably well described by the first σ - σ crossing, but the dominance of $3p$ excitation is still not obvious at this stage of the calculation. It is interesting, however, to examine the results obtained by Kempter²⁸ on the energy dependence of the total cross section for the $3p'$ - $3s$ (6280 Å) optical transition observed in Ne-Ne collisions. This cross section is linearly dependent on beam energy below 300 eV and thus easily provides the energy threshold: 97 eV. The threshold for the primary X - C crossing occurs at a laboratory en-

ergy of 96.4 eV (48.2 eV in the c.m. system shown in Fig. 11) as calculated by the *ab initio* techniques. This is, of course, the minimum kinetic energy required to reach the crossing. The agreement in threshold energy between theory and experiment is seen to be quite good. As additional confirmation the Ne-Ne ionization studies of Amme and Haugsjaa²⁹ yield a laboratory energy threshold energy of about 103 eV which is also in reasonable agreement with the present calculations.

The agreement (angular and energy thresholds, phase oscillations, and relative cross-section magnitudes) are strong arguments for the dominance of the $4f\sigma_u-3s\sigma_g$ MO crossing effects in lieu of the $4f\sigma_u-3p\pi_u$ rotational coupling in spite of the marked $3p$ excitation. It is also important at this time to determine the energy threshold associated with the next inner $\Sigma-\Sigma$ crossing to definitely establish the primary excitation mechanism. This crossing occurs between the incident channel and the (core) $3\sigma_g^2 4\sigma_g 5\sigma_g$ molecular configuration. We estimate that the laboratory threshold energy associated with this crossing is 111 eV and conclude that the C state is indeed responsible for the observed threshold. The incident X channel also crosses the other curves of the C series leading to similar excitation mechanisms which do contribute to the scattered signal. However, the primary interactions with these higher-lying states are expected to be weaker.

Up to now we have studied in detail only the effect of the first $3\sigma_u-4\sigma_g$ MO crossing (Fig. 10). At closer internuclear distance we must also consider the effect of the $3\sigma_u-4\sigma_u$ MO pseudocrossing where one- or two-electron transitions are allowed and lead to crossings between the incident diabatic potential curve and diabatic potential-energy curves generated in both the A series and the D series ($3\sigma_g^2 4\sigma_u n\sigma_u$, $n \geq 4$; see Fig. 11). In this same region (internuclear separation about 1.6 bohr) the incident channel can also couple (directly and indirectly) with the $^1\Sigma_g^+$ and (indirectly) with the $^1\Delta_g$ states arising from two-electron excitation of the $2\pi_u$ MO. This region is, in fact, too crowded to be examined in detail at this time. The location of the first maximum in the experimental reduced cross sections, however, for $2\text{Ne}(2p^5 3p)$ excitation ($\tau \approx 6.5$ keV deg) corresponds to a crossing point at about 1.6 bohr (determined by trajectory calculations) confirming the importance of the region. This very crowded region is also responsible for the severe loss in the elastic channel and the wide broadening of the two-electron excitation peak. The direct coupling of the incident channel with the continua contributes to these effects. Evidence for this direct coupling with the continua can be found by examining the position of the maximum in the

C' ionization peak as a function of τ (Fig. 13). The ionization probability is expected to attain its maximum value at the turning point of the trajectory since the radial velocity vanishes there. As the collision becomes harder (larger τ values) the turning point moves in and consequently leads to larger energy losses. The expected value of the energy loss as a function of τ has been calculated

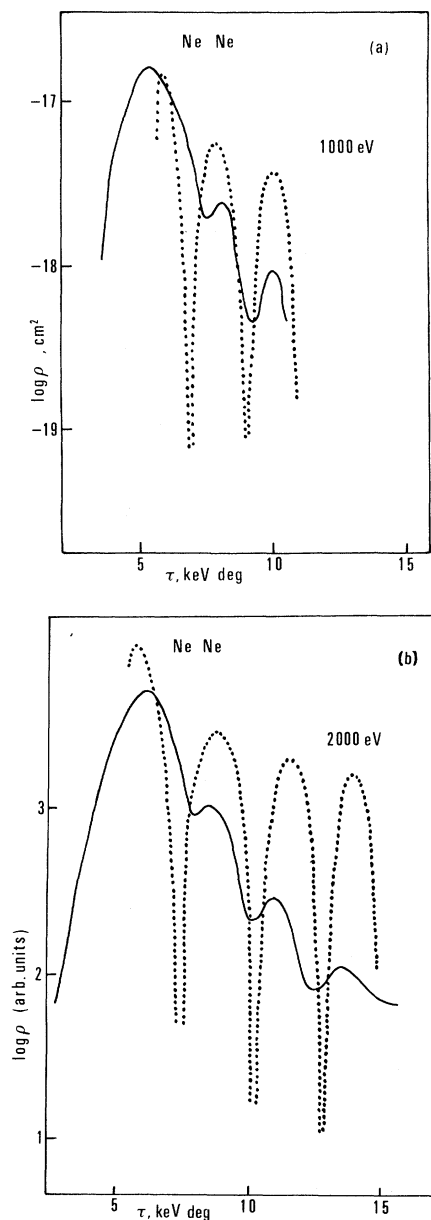


FIG. 12. Comparison of the theoretical (dotted line) and experimental (full line) differential cross sections for (a) single excitation (peak B), and (b) simple ionization at threshold (peak B').

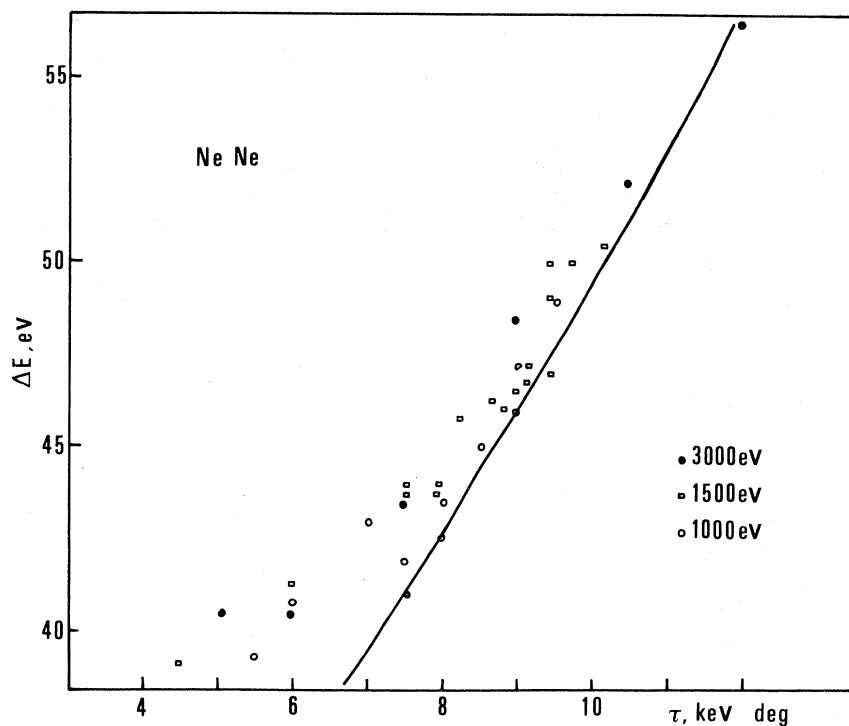


FIG. 13. Position of the maximum of the C' ionization peak in Ne-Ne as a function of the reduced scattering angle. The full line is the theoretical result obtained from the assumed model and is in reasonable agreement with the experimental points.

using the incident diabatic channel and a potential suitably shifted from that associated with the $3\sigma_g^2 4\sigma_g \text{Ne}_2^+$ continuum configuration. These results are also plotted in Fig. 13 and show good agreement at large τ with a worsening agreement near threshold tentatively attributed to tunneling effects.

It is interesting to compare results obtained by integrating the experimentally determined differential cross section for ionization with the measured total cross section for ionization as reported by Amme and Haugsjaa.²⁹ In addition using the LZS approximation we have calculated the energy dependence of the total cross section arising from the $X-C$ crossing. The results are presented in Fig. 14 and compared with the sum of the single excitation and simple ionization total cross sections. At 1 keV the experimental results are higher than the theoretical results by a factor of 2.3 and indicate the inadequacy of the model. A comparison of the optical-excitation results²⁸ with the ionization results of Amme²⁹ (Fig. 14) shows a striking similarity of threshold behavior and shape which is not surprising in view of the model. On the other hand, the agreement in shape is not reproduced by the calculation involving the $X-C$ crossing. It is clear that processes coming from inner crossings should not be neglected in refined calculations.

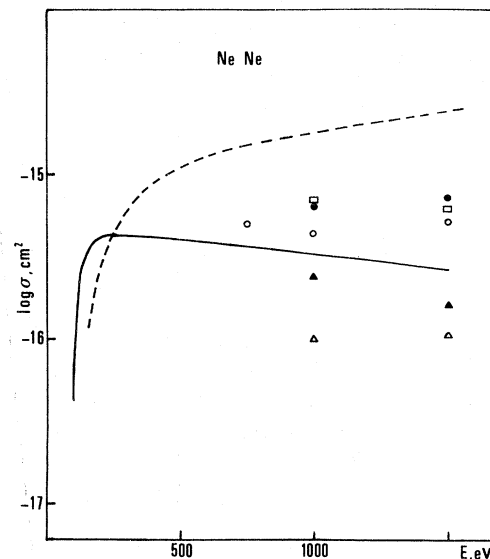


FIG. 14. Total cross sections, for some processes in Ne-Ne collisions, as a function of laboratory energy. The points are obtained by integrating the present experimental differential cross sections. Open triangle: simple ionization (peak B'); full triangle: ionization with target excitation (peak C' : $Q=42.5$ eV); open circles: single excitation (peak B); full circles: sum of single excitation and single ionization (to be compared with the theoretical cross section, shown in full line resulting from the $X-C$ crossing); rectangle: sum of the cross sections for ionizing processes ($B' + C'$) [to be compared with the experimental results of Amme (Ref. 29) shown by the dashed curve].

B. Ar-Ar collision

1. Spectra and cross sections

The Ar-Ar collision is studied in the energy range from 0.75 to 4.0 keV. Figure 15 shows typical energy-loss spectra of the scattered Ar. For both low energy and small- τ values the resolution is sufficiently good to demonstrate that inelastic processes are due mainly to the excitation of $4s$ and $4p$ levels. At higher energies the location of the peak maximum oscillates between the $4p$ position and positions corresponding to higher excited levels. This behavior suggests an underlying oscillatory reduced cross sections for the processes involved. The peak corresponding to two-electron excitation processes (C) is located at an energy loss corresponding to the excitation of $2 \text{ Ar}(3p^5 4s)$ for $\tau \lesssim 4 \text{ keV deg}$. At larger τ values, peak C broadens to include contributions from $2 \text{ Ar}(3p^5 4p)$ and from higher excited levels. The Ar^+ spectra⁸ from these collisions show that doubly excited autoionizing levels are also present. For $\tau > 25 \text{ keV deg}$ two additional peaks, corresponding to average energy losses of 40 to 45 eV for one of the peaks and losses greater than 60 eV for the other, are found.

Figure 16 shows the cross sections for several processes. At a given energy the elastic cross

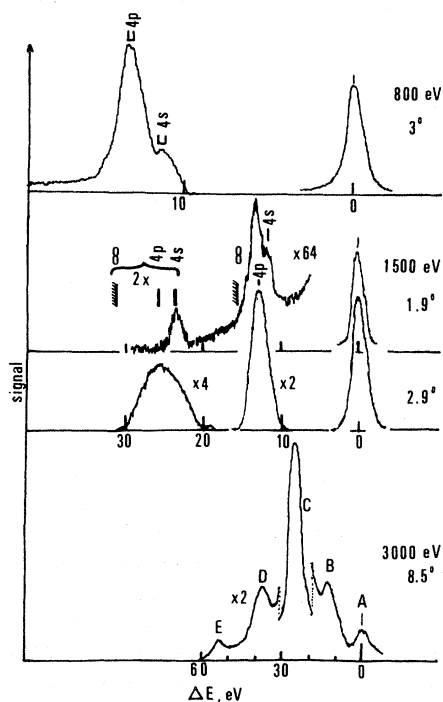


FIG. 15. Energy-loss spectra of scattered Ar from Ar-Ar collisions. The same notation is used as in Fig. 1.

section (ρ_A) is seen to fall sharply with increasing τ . The curves also exhibit an increasing sharpness in their fall off as the energy increases. As has been previously found this rapid decrease signals the onset of inelastic processes. The elastic channel however recovers at sufficiently large τ values as expected in a strong absorption.³⁰ The one-electron excitation cross sections (ρ_B) shown

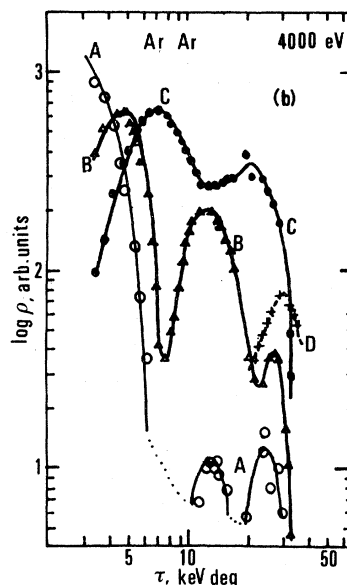
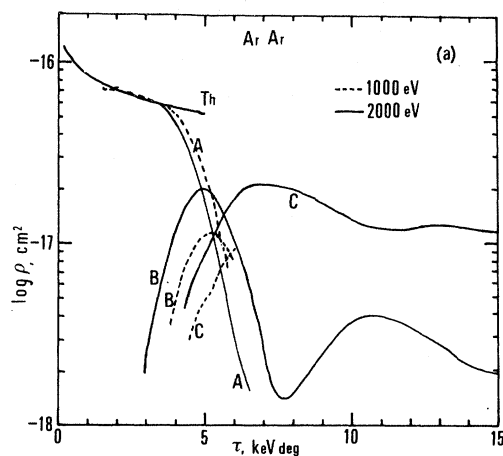


FIG. 16. Reduced differential cross sections for Ar-Ar collisions as a function of τ , the reduced scattering angle. The same notation is used as in Fig. 3. (a) Results are normalized to theory at small angle. (b) Unnormalized reduced cross sections at a 4.0-keV laboratory energy over a large range of τ values. The elastic peak A is seen to exhibit a "diffraction" pattern in the region of strong absorption. Peaks B and C are seen to oscillate out of phase. The minimum separation (at $\tau = 12 \text{ keV deg}$) between B and C is found to decrease rapidly with increasing energy. At large τ values (30 keV deg) process D is seen to dominate.

do not display the fast Stueckelberg oscillations evident in Ne-Ne (where the excitation more selectively involves the $3p$ level) since the resolution allows cross sections determinations to be made only from the height of the peak generated by the combined one-electron processes. At values of τ beyond the triple-peak region ($\tau=5.5$ keV deg) a second and broader peak (for the one-electron processes) appears and has its maximum value for $\tau > 10$ keV deg. As may be seen, the two-electron excitation processes (ρ_C) exhibit a broad maximum followed by a minimum located at the position of the second maximum in the one-electron excitation cross sections. The separation between ρ_B and ρ_C in this region decreases rapidly with increasing energy. At high energy the process ρ_D

(Q about 40 to 45 eV) is found dominant near $\tau=30$ keV deg.

2. Ar-Ar discussion

The Ar + Ar system is analyzed in a manner similar to that employed in the Ne + Ne case. We calculate potential energy curves and electronic wave functions for $31\ ^1\Sigma_g^+$, two $^1\Pi_g$, and six $^1\Delta_g$ states obtained in the virtual-orbital approximation, using the $\text{Ar}_2^+ X\ ^2\Sigma_u^+$ reference state³¹ and the same calculation technique as employed for the Ne + Ne system. The configurations considered here as well as their dissociation products are listed below:

$$\begin{array}{l}
 R \rightarrow \infty \\
 \left. \begin{array}{l} 5\sigma_g^2 5\sigma_u^2 \\ 5\sigma_g^2 5\sigma_u n\sigma_u \\ 5\sigma_u^2 5\sigma_g n\sigma_g \end{array} \right\} \left\{ \begin{array}{l} \text{Ar}(3p^6) + \text{Ar}(3p^6) \\ \text{Ar}(3p^5 4s \text{ or } 4p) + \text{Ar}(3p^6) \\ \text{Ar}^-(3p^6 4s \text{ or } 4p) + \text{Ar}^+(3p^5) \end{array} \right. \\
 \left. \begin{array}{l} 5\sigma_g^2 n\sigma_g m\sigma_g \\ 5\sigma_g^2 n\sigma_u m\sigma_u \\ 5\sigma_u^2 n\sigma_g m\sigma_g \\ 5\sigma_u^2 n\sigma_u m\sigma_u \\ 5\sigma_g 5\sigma_u n\sigma_g m\sigma_u \end{array} \right\} \left\{ \begin{array}{l} \text{Ar}(3p^5 4s \text{ or } 4p) + \text{Ar}(3p^5 4s \text{ or } 4p) \\ \text{Ar}^{2-}(3p^6 4s^2 \text{ or } 4s 4p \text{ or } 4p^2) + \text{Ar}^{2+}(3p_\pi^4) \\ \text{Ar}^-(3p^6 4s \text{ or } 4p) + \text{Ar}^+(3p_\pi^4 4s \text{ or } 4p) \\ \text{Ar}(3p_\pi^4 4s^2 \text{ or } 4s 4p \text{ or } 4p^2) + \text{Ar}(3p^6) \\ \text{Ar}^-(3p^5 4s^2 \text{ or } 4s 4p \text{ or } 4p^2) + \text{Ar}^+(3p^5) \end{array} \right. \\
 (n=6, 7; m=6, 7) \\
 \left. \begin{array}{l} 5\sigma_g^2 5\sigma_u 3\pi_u \\ 5\sigma_u^2 5\sigma_g 3\pi_g \end{array} \right\} \left\{ \begin{array}{l} \text{Ar}(3p^5 4p) + \text{Ar}(3p^6) \\ \text{Ar}^-(3p^6 4p) + \text{Ar}^+(3p^5) \end{array} \right. \\
 \left. \begin{array}{l} 5\sigma_g^2 3\pi_u^2 \\ 5\sigma_g^2 3\pi_g^2 \\ 5\sigma_u^2 3\pi_u^2 \\ 5\sigma_u^2 3\pi_g^2 \\ 5\sigma_g 5\sigma_u 3\pi_u 3\pi_g \end{array} \right\} \left\{ \begin{array}{l} \text{Ar}(3p^5 4p) + \text{Ar}(3p^5 4p) \\ \text{Ar}^-(3p^6 4p) + \text{Ar}^+(3p_\pi^4 4p) \\ \text{Ar}(3p_\pi^4 4p^2) + \text{Ar}(3p^6) \\ \text{Ar}^{2-}(3p^6 4p^2) + \text{Ar}^{2+}(3p_\pi^4) \\ \text{Ar}^-(3p^5 4p^2) + \text{Ar}^+(3p^5) \end{array} \right.
 \end{array}$$

To ensure the proper dissociations (symmetric, asymmetric, covalent, or ionic), configuration-interaction calculations, in particular for $R > 3$ bohr, are made for these states.

The determination of the incident diabatic potential-energy curve requires a knowledge of the diabatic MO's. Although the problem associated with the calculation of such MO's is open, as mentioned earlier, a few methods have been proposed to deal with it.^{6,25,31} The technique used here consists in deleting from the atomic LCAO expansion

basis all excited orbitals (as an example for $\text{Ar}_2: 4s, 4p, 3d$, etc.) in order to avoid the mixings responsible for MO pseudocrossings. Using this approximation, we obtain the diabatic $X\ ^1\Sigma_g^+$ incident state potential shown in Fig. 17. Selected numerical values of the potential for the "ground" state are compared with those of other authors³² in Table III. The computed single-configuration potential-energy curves for some excited states are also shown in Fig. 17 (note the similarity to the Ne₂ case in Fig. 11). This figure displays an

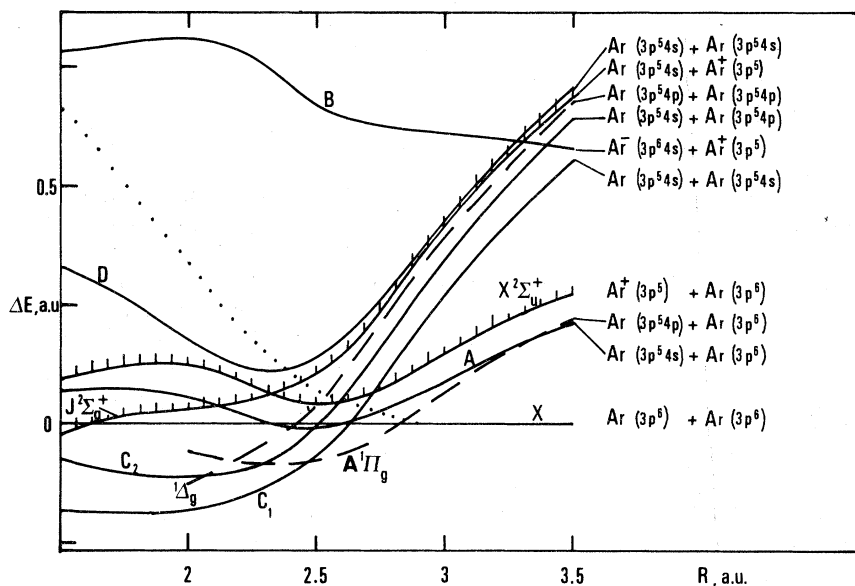


FIG. 17. Several potential-energy curves for Ar_2 and Ar_2^+ referred to the $X^1\Sigma_g^+$ (core) $5\sigma_g^2 5\sigma_u^2$ level. The estimated incident diatomic channel corresponding to the $5f\sigma_u$ promotion is represented by the dotted curve.

analogous pinching between the $X^1\Sigma_g^+$ and $X^2\Sigma_u^+$ states which contains all the curves arising from the singly excited configurations $5\sigma_g^2 5\sigma_u n\sigma_u$ ($n > 5$). As in the Ne_2 case, the $X^1\Sigma_g^+$ curve crosses an infinite number of quasidiatomic curves (C series). The (core) $5\sigma_g^2 6\sigma_g^2$ and (core) $5\sigma_g^2 6\sigma_g 7\sigma_g$ curves which are the two lowest in the C series are shown along with the corresponding (core) $5\sigma_g^2 6\sigma_g$ excited continuum curve. As previously noted this set of crossings arises from promotion of the $5\sigma_u$ MO (this orbital originates from $\sigma_u 3p_{\text{Ar}}$ and evolves to the $5f\sigma_{u\text{Kr}}$) leading to subsequent σ_u - σ_g crossings with the first being $5\sigma_u$ - $6\sigma_g$ ($5f\sigma_u$ - $4s\sigma_g$). The promoted $5\sigma_u$ MO in addition avoids crossings with higher-lying σ_u MO's. It is reasonable to attribute the shapes of the curves in the A series and also

in the D series to these avoided crossings. The region of crossings discussed above and lying between 2 and 3 bohr is responsible for much of the single excitation, ionization, and symmetrical excitation in the triple-peak region ($\tau \approx 5$ keV deg). It is interesting at this point to look at the experimental results on the total cross sections for uv^{33} emission and electron ejection in $\text{Ar} + \text{Ar}$ collisions.³⁴ The experimental results suggest an energy threshold of 30 eV, in the c.m. system, for these processes (see $\text{Ne}-\text{Ne}$ discussion above) which is in agreement to within a few eV with our value of 31 eV for the energy value at the $X^1\Sigma_g^+$ - $C(5\sigma_g^2 6\sigma_g^2)$ crossing. Calculations of the location of the X - $A^1\Pi_g$ crossing position ($R_X \approx 2.9$ bohr, $V \approx 24.6$ eV in c.m.) clearly show that this

TABLE III. A comparison between some "ground-state" potentials for Ar_2 : (a) the present results obtained in the virtual orbitals approximation using the $X^2\Sigma_u^+$ state of Ar_2^+ (Ref. 31) and (b) the ground incident diatomic potential. GW, S, GK have the same meaning as in Table II. A are the results of Abrahamson (Ref. 32) and BM the results Bellum and Micha (Ref. 32).

R	(a)	(b)	GW	A	S	GK	BM
1	29.2592	37.5421	60.7239	24.57	...
1.5	9.6596	10.2800	...	14.3817	21.6024	7.229	...
2	3.4781	3.8245	...	5.5094	7.6850	2.301	...
2.5	1.5715	1.6362	...	2.1105	2.7339	...	2.4594
3.	0.7456	0.7456	0.7142	0.8085	0.9725	0.3946	1.1537
3.5	0.3352	0.3352	...	0.3097	0.3460	...	0.5412
3.8	0.1908	...	0.1861	...	0.3437
4	0.1351	0.1187	0.1231	0.0757	0.2539
4.2	0.0953	...	0.0814	...	0.1876
4.5	0.0838	0.0838	...	0.0454	0.0438	...	0.1191
4.6	0.0467	...	0.0356	0.0247	0.1024
4.7	0.0389	0.0880
5	0.0224	0.0174	0.0156	0.0107	0.0559

mechanism is unable to account for the above experimental energy threshold. In addition, the results of Kempter and Zehnle²⁸ concerning the excitation of the $5p$ level indicate a threshold at 35 eV. As in the Ne_2 case the convergence of the threshold values for both single excitation and ionization points to a common primary mechanism involving the X - C crossing followed by C - A series crossings. Of course, all higher states of the doubly excited C series also contribute to these processes. As in Ne-Ne the next excitation mechanisms would involve the $5\sigma_u$ - $6\sigma_u$ avoided MO crossing which directly populates the D series. This mechanism is thought to be responsible for a second threshold, observed by Kempter and Zehnle²⁸ for the $5p$ excitation, corresponding to an energy of about 56 eV in the c.m. Our estimate for this threshold lies at 58 ± 2 eV (see Fig. 17). In harder collisions the problem becomes more complex (see Ne-Ne discussion). The present differential-scattering results on Ar-Ar are discussed in the framework of the above model. As in the Ne-Ne case we have calculated the differential cross sections assuming first the participation of only the lowest crossing in the X - C series. The participation of the X - A $^1\Pi_g$ interaction (rotational coupling) was previously rejected on energy-threshold arguments. Furthermore, calculations of τ corresponding to this crossing leads to a value of 3.3 keV deg, which is less than the experimentally determined value of about 4.7 keV deg, for the position of the first maximum of the inelastic reduced cross sections. Coming back to the effective mechanism (X - C crossing), the maximum of the theoretical reduced cross sections for single excitation occurs at $\tau = 4.6$ keV deg in good agreement with the experimental results. However, the frequency of the Stueckelberg oscillations in the theoretical reduced cross sections (≈ 1.5 keV deg) is too high to account for the shape of the experimental cross section. To study the effect of additional crossings in the X - C series on the reduced cross section we investigate the effect of the inclusion of eight states in a LZS JWKB approach.³⁵ In this case the elastic reduced cross sections shows the marked falloff (by one to two orders of magnitude in the τ region between 5 and 8 keV deg) due to the absorption in the inelastic channels. The experimental elastic reduced cross sections shown in Fig. 16 display a much stronger falloff starting at a smaller τ value. The limited calculations performed, however, do account for the order of magnitude of the measured one- and two-electron excitation reduced cross sections.

As additional confirmation of the primary mechanism, the differential measurements of Eriksen

*et al.*⁸ show that ionizing processes become important at τ values of about 5 keV deg. Ionization resulting from two-electron excitation (energy loss of about 30 eV) was found to be the dominant process below $\tau \approx 24$ keV deg. At $\tau \approx 30$ keV deg the ion peak, however, lies at about a 43 eV loss. An analogous peak (D) is seen in our neutral spectrum at about 30 keV deg. Furthermore, a similar peak was seen in the $\text{Ar}^+ + \text{Ar}$ case.²⁰ This new process occurring both in the neutral and ionic systems for similar values of τ is not related to the $5f\sigma_u$ MO promotion responsible for the triple-peak region but arises from additional crossings at smaller values of the internuclear separation. Although there are several processes that can account for a 43-eV loss it is reasonable to assume that three-electron processes (involving at least a two-step mechanism) would be weak. The only possibility is one involving a two-electron transition from the $3s$ and $3p$ levels either in one or both atoms.⁸

The ejected electron energy spectra¹⁴ show a peak at 9.4 eV attributable to the excitation of Ar ($3s3p^64s$). The excitation function for this process has a threshold at 42 eV (c.m.) which is also explainable by our potential-energy curves. Indeed, the $\text{Ar}(3s3p^64s) + \text{Ar}$ level lies in the lower part of the energy range corresponding to $\text{Ar}(3p^5nl) + \text{Ar}(3p^5nl')$ and is excitable through a two-step process. The mechanism again involves the primary X - C interaction followed by subsequent crossing with the more repulsive state arising from $\text{Ar}(3s3p^64s) + \text{Ar}(3p^6)$. However, the first X - C crossing [leading to $2\text{Ar}(3p^54s)$] cannot account for the process since the C curve responsible for the symmetric excitation cannot cross the $^1\Sigma_g^+$ curve arising from $\text{Ar}(3s3p^64s)$ and, indeed lies 2 eV below this level at infinite separation. However, inner X - C crossings can be effective. Such crossings occur for internuclear separation of about 2.5 bohr and correspond to an energy threshold of about 40 ± 3 eV (c.m.) in agreement with the observed value.

C. Kr-Kr collisions

The Kr-Kr case is studied at only 2 and 3 keV to verify the promotion of one or two electrons from the $6h\sigma_u$ MO. Here also the spectra display the three peaks. Cross sections at 3 keV are shown in Fig. 18. The behavior is very similar to that in the previous cases and shows that the promotion occurs at a τ value of about 9 keV deg.

IV. CONCLUSION

The Fano-Lichten promotion model has successfully explained inner-shell excitation, particularly

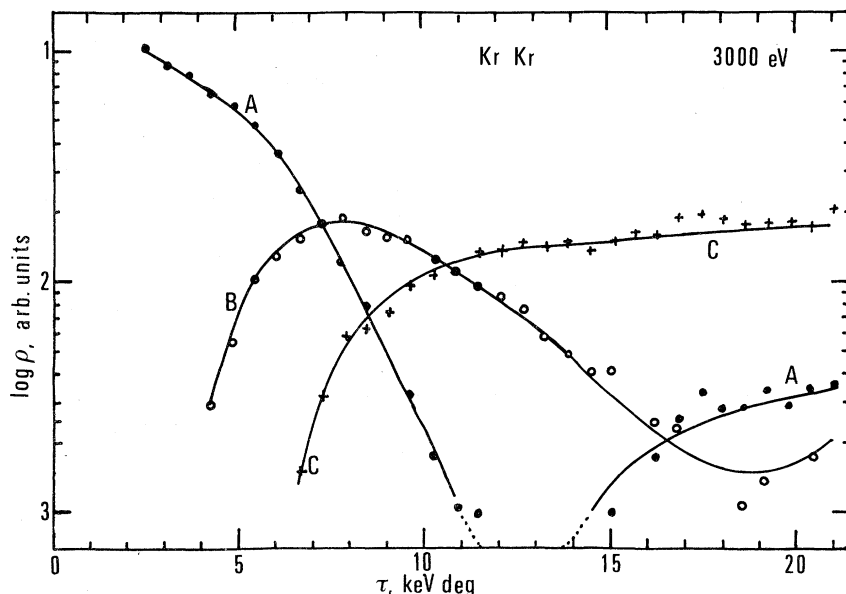


FIG. 18. Reduced differential cross sections as a function of reduced scattering angle for Kr-Kr collisions. The same notation is used as in Fig. 3. The triple-peak behavior occurs at a reduced angle of about 8.5 keV deg. The recovery of the elastic channel is also seen.

for the well-known Ar⁺-Ar and Ne⁺-Ne systems. We have shown in this work that the same approximations hold for outer-shell processes in similar symmetric systems.

In the simple H₂⁺-like model one- or two-electron excitation can occur at the crossing of a filled σ MO with empty MO's. For instance, K -shell excitation is induced by the $2p\sigma_u-2p\pi_u$ rotational coupling leading to an inner- K -shell vacancy in Ne-Ne collisions and also to selective $2p$ excitation in He⁺+He and in He+He.

Excitation of electrons from L shells occurs via the $4f\sigma_u$ promotion in the inner shell for Ar+Ar or outer shells for the Ne-Ne and Ne⁺+Ne cases. M -shell excitation occurs similarly through the $5f\sigma_u$ MO in the Ar+Ar and Ar⁺+Ar cases. In the case of Kr the M -shell excitations proceed through the promoted $6h\sigma_u$ MO, whereas the outer N shell is excited through the promoted $6f\sigma_u$. Since the same correlation diagram is applicable to both the ion-atom and atom-atom systems it is interesting to compare the triple-peak region in the ionic and atomic cases. The experimental results to date show a similar behavior, at τ values of several keV deg of the reduced cross sections. The mechanism involved here (i.e., MO promotion) is therefore thought to be common to many heavy-particle systems and is primarily responsible for excitation in the low-keV energy range (1–10 keV).

An analysis of the present experimental results reveals the striking weakness for the excitation of the first excited state (ns) in contrast with the importance of the next-higher-lying state involving p electrons. These selective p excitation processes were expected to arise from rotational

coupling, as is indeed the case in He-He. However, for heavier systems the current theoretical arguments do not support this mechanism. The σ - σ interactions are, however, able to explain most of the observed features except that the dominance of p excitation is not yet well understood.

Although the previous discussion based on the MO picture provides a simple model enabling a qualitative understanding of the collision, it should be emphasized that only the molecular *states* (describing the entire electronic system) are actually involved in the collision problem. Each MO crossing discussed above generates several crossings of the molecular-potential energy curves (see the Appendix) in a single-configuration picture (diabatic I). Considering the general case of a filled and promoted incident orbital (A) crossing an initially empty MO (B), one- or two-electron transitions from A to B leads to the first generated crossings of the states corresponding to the A^2 , AB , and B^2 configurations. If A and B are of different u, g symmetry, only transitions from A^2 to B^2 are allowed. In addition the same A - B MO crossing may lead to an infinite number of state crossings A^2 - BC (where C is an empty MO lying above B and not necessarily crossing A). Of course the continuum can be included (A^2 - $B+\bar{e}$). In summary, processes termed diabatic I require at least one MO crossing. A second category of diabatic-state crossings not related to any MO crossings are also found (diabatic II). This situation arises when a vacancy is initially present in an MO which is less promoted than the outer filled ones. Such "core-excited" configurations generally result in incident states which are highly

repulsive and correlate to autoionizing states of the united atom. As a consequence this state *must* cross the infinite series of singly excited states having a lower-core excitation. These diabatic II processes arise especially in rare-gas ion on rare-gas collisions and are in fact responsible for the importance of inelastic processes at low energy³⁶ (tens of eV). The absence of the initial core vacancy in the neutral system and consequently of diabatic II processes make the dramatic

difference in the behavior of neutral and ionic system at low energies. The He⁺+He case, which has received a great deal of attention, provides the typical example in which the diabatic-II inelastic processes involve the initial $1s\sigma_g 2p\sigma_u^2(^2\Sigma_g^+)$ state interacting with $1s\sigma_g^2 n l\sigma_g(^2\Sigma_g^+)$ states. In addition all other symmetric rare-gas ionic systems exhibit either Σ - Σ or Π - Π diabatic-II processes depending on whether a σ or π MO vacancy exists initially.³¹ Usually the diabatic-II-type

TABLE IV. Summary of the known inelastic-scattering mechanisms and characteristics associated with symmetric rare-gas collision systems. In each case the participating MO's are identified, the theoretical value of the crossing positions (R) are given in bohrs (at least for the outermost crossing), and the experimentally determined τ (reduced scattering angles) values are given in units of keV deg. $R = 0$ refers symbolically to rotational coupling in the united atom.

		Diabatic II		Diabatic I (outer shell)		Diabatic I ^a
		Σ - Σ coupling	Π - Π coupling	σ - σ coupling	Rotational coupling	inner shell
He	He ⁺ -He	$2p\sigma_u^2-1s\sigma_g n l\sigma_g$ $R = 1.5-1.2$ $\tau = 0.6-1.2$ Refs. b, c	Not present	$2p\sigma_u-2s\sigma_g$?	$2p\sigma_u-2p\pi_u$ $R = 0$ $\tau \approx 3$	Refs. l, c
	He-He	Not present	Not present	$2p\sigma_u-2s\sigma_g$ $R \approx 0.5$ Refs. d, e	$2p\sigma_u-2p\pi_u$ $R = 0$ $\tau \approx 2-3$	Refs. d, f
Ne	Ne ⁺ -Ne	$4f\sigma_u^2-3d\sigma_g n l\sigma_g$ $R \leq 2.3$ Ref. g	$4f\sigma_u 3d\pi_g-2p\pi_u n l\sigma_g$ $R \leq 2.1$ Ref. g	$4f\sigma_u-3s\sigma_g, \dots$ $R \leq 1.65$ $\tau \approx 10$ Refs. g, h	$4f\sigma_u-3p\pi_u$	$2p\sigma_u-2p\pi_u$ $R = 0$ $\tau \sim 1500$
	Ne-Ne	Not present	Not present	$4f\sigma_u-3s\sigma_g, \dots$ $R \leq 1.8$ $\tau \approx 5.5$ Ref. f	$4f\sigma_u-3p\pi_u$ $R \leq 1.6-1.9$ very weak Ref. f	Ref. i
Ar	Ar ⁺ -Ar	$5f\sigma_u^2-4d\sigma_g n l\sigma_g$ $R \leq 3.6$ $\tau \approx 0.65$ Ref. j	$5f\sigma_u 4d\pi_g-3p\pi_u n l\sigma_g$ $R \leq 3.1$ $\tau \approx 2.3$ Ref. j	$5f\sigma_u-4s\sigma_g, \dots$ $R \leq 2.3$ $\tau \approx 7$ Refs. h, j	$5f\sigma_u-3p\pi_u$ $R \leq 2.1$	$4f\sigma_u$ $R \approx 0.6$ $\tau \sim 400$
	Ar-Ar	Not present	Not present	$5f\sigma_u-4s\sigma_g$ $R \leq 2.7$ $\tau \approx 5$ Ref. k	$5f\sigma_u-3p\pi_u$ $R \leq 2.55-2.9$ very weak Ref. k	Refs. i, j

^aOther intermediate MO crossings between those listed for outer and inner shells are also present although their effects are not yet well understood.

^bReference 36.

^cM. Barat, D. Dhucq, R. François, R. McCarroll, R. D. Piacentini, and A. Salin, *J. Phys. B* **5**, 1343 (1972).

^dReference 7.

^eJ. C. Bellum and D. A. Micha, *Int. J. Quantum Chem.* (to be published).

^fPresent work.

^gReference 25 and present work.

^hReferences 19 and 20.

ⁱReferences 1, 2, and 18 in text.

^jReference 31.

^kReference 8 and present work.

^lR. McCarroll and R. D. Piacentini, *J. Phys. B* **4**, 1026 (1971).

crossings occur at larger internuclear distances than those associated with the diabatic-I type. Figure 19 summarizes the typical characteristics associated with the various diabatic processes and emphasizes the marked differences between the ionic and neutral symmetric systems (at small τ values). The known characteristics of the symmetric rare-gas systems are presented in Table IV. From the theorist's point of view the treatment of the diabatic-II cases is usually simpler than for diabatic-I cases since the d/dR operator between the type-II states (quasidiabatic) is zero.^{11,21} The only effective couplings which need be considered are interelectronic-electrostatic interactions. These interactions are usually small (≤ 1 eV) and thereby allow the treatment of inelastic processes as small perturbations which only slightly affect the elastic scattering. The first crossing of the infinite series of diabatic-II crossings is usually well separated from the others and has become the war-horse of simplified treatments such as the two state LZS approximation or more sophisticated approaches.³⁷ In the diabatic-I category one may still distinguish between two types of MO crossings depending on whether the MO's have the same symmetry (u, g) or not. For

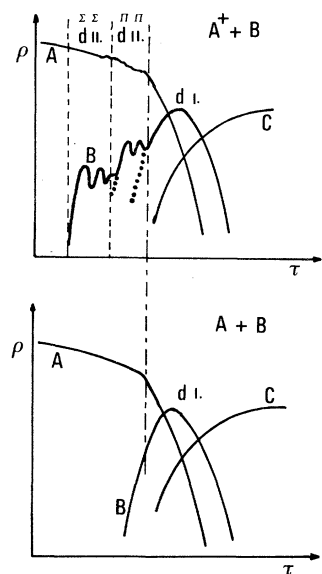


FIG. 19. Schematic comparison of the expected behavior of the elastic (A), one-electron (B), and two-electron (C) cross sections for the ionic and neutral scattering systems. At medium τ values both systems are expected to exhibit a similar triple-peak behavior arising from the same MO crossing (diabatic I— dI). In the ionic system the presence of diabatic II (dII) processes causes additional inelastic scattering via Σ - Σ or Π - Π interactions, at smaller τ values. Such crossings are generally well localized and give rise to Stueckelberg oscillations in the scattering pattern.

the case where the symmetries are different, only two-electron transitions are allowed and the quasidiabatic treatment discussed above is applicable (see section on Ne_2). If the symmetries are the same, the problem becomes more difficult and remains as yet an outstanding one. In the present state of the theory Hartree-Fock-type calculations are used and yield avoided MO and state crossings. The couplings between states in this approach come from the electronic Hamiltonian (\approx few eV, except for the Brillouin theorem²⁶) and the d/dR operator. The resulting problem involves at least a three-state approximation (as an example A^2 - AB - B^2 in the previous notation). In using electronic wave functions describing a single configuration of Hartree-Fock MO's, the treatment of the pseudocrossing region necessitates the computation of d/dR matrix elements which is difficult or expensive. A more attractive approach would consist in finding a practical definition which allows a direct calculation and simple use of diabatic MO's. A tentative method could start from the ideas of Smith¹¹ together with the suggested "node-conservation rule" of Barat and Lichten.³⁸ As another suggestion this problem can be handled by using pseudopotentials. Since two electrons are active ($4f\sigma_u^2$ in Ne-Ne), a model with two electrons in the field of an effective core could provide (for the internuclear separations of

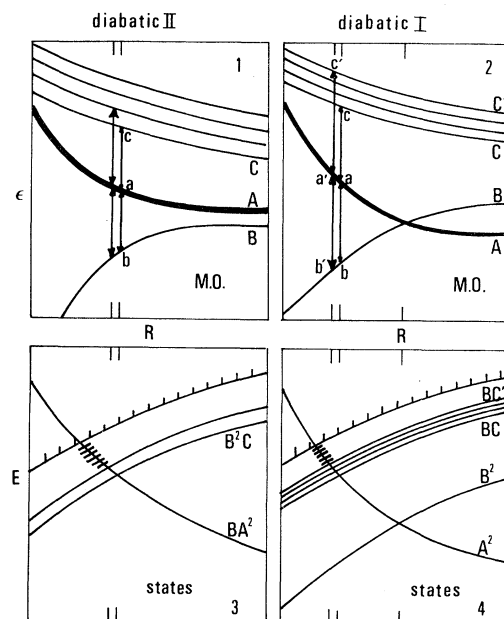


FIG. 20. Schematic representation showing the large number of state curve crossings generated by an inner MO vacancy. In the diabatic-II case the vacancy is initially present in B while in diabatic-I processes a vacancy may be created at an MO crossing. In both cases A is filled.

interest) appropriate electronic wave functions.

Even if we assume that this goal can soon be attained, the available experimental results show that diabatic-I crossings lead to the simultaneous opening of many inelastic channels and as a consequence the theoretical treatment of such problems can be approached either qualitatively or by using approximate models for dealing with large numbers of coupled states.

APPENDIX

A series of quasidiabatic state crossings is generated when a vacancy is present in an inner MO. In some cases (rare-gas ion-rare-gas atom) this vacancy is *initially* present in the system and the resulting crossings are called diabatic II. This condition is shown in Fig. 20(a). In the general

case (diabatic I) the inner vacancy is created at a crossing of an initially filled and promoted MO with an empty MO [Fig. 20(b)]. If we now consider higher excited empty MO's [Fig. 20(a) and (b)] in both cases the condition required for state crossings is $2\epsilon_A - (\epsilon_B + \epsilon_C) = 0$, where ϵ is the MO energy. This condition is generally fulfilled since the C, C', \dots orbitals are very weakly bound with respect to the binding energy of B (see Fig. 20). In both cases an infinite series of quasidiabatic crossings is generated. The above argument is valid only under the simple assumption that the total electronic energies is the sum of the MO energies. If proper account is taken of the necessary Coulomb and exchange terms, the basic argument remains the same, there are only shifts in the energies and crossing positions.

*Permanent address: Dept. of Physics, University of Connecticut, Storrs, Conn. 06268. Collaboration made possible by NATO under Grant No. 736 and the University of Connecticut Research Foundation.

†Equipe de recherche du Centre National de la Recherche Scientifique.

¹U. Fano and W. Lichten, *Phys. Rev. Lett.* **14**, 627 (1965).

²W. Lichten, *Phys. Rev.* **164**, 131 (1967).

³J. E. Jordan and I. Amdur, *J. Chem. Phys.* **46**, 165 (1967); I. Amdur, J. E. Jordan, and R. R. Bertrand, in *Atomic Collision Processes*, edited by M. R. C. McDowell (North-Holland, Amsterdam, 1964), p. 934; S. O. Colgate, J. E. Jordan, I. Amdur and E. A. Mason, *J. Chem. Phys.* **51**, 968 (1969); I. Amdur and E. A. Mason, *J. Chem. Phys.* **23**, 415 (1955); see also Smith Ref. 32.

⁴D. C. Lorents and G. M. Conklin, *J. Phys. B* **5**, 950 (1972); R. François, D. Dhucq, and M. Barat, *ibid.* **5**, 963 (1972); C. Lesech, R. McCaroll, and J. Baudon, *ibid.* **6**, L11 (1973); V. V. Afrosimov, Yu. S. Gordeev and V. M. Lavrov, *Zh. Eksp. Teor. Fiz. Pisma Red.* **16**, 480 (1972) [*JETP Lett.* **16**, 341 (1972)]; Z. Z. Latypov and A. A. Shaporenko, *Zh. Eksp. Teor. Fiz.* **63**, 1300, (1973) [*Sov. Phys.—JETP* **18**, 824 (1973)].

⁵V. V. Afrosimov, Yu. S. Gordeev and V. M. Lavrov, in *Eighth International Conference on the Physics of Electronic and Atomic Collisions (Abstracts of Papers)*, edited by B. C. Cobic and M. V. Kurepa (Institute of Physics, Belgrade, 1973), Vol. 1, p. 190; V. V. Afrosimov, Yu. S. Gordeev, V. M. Lavrov, and V. K. Nikulin, in *Seventh International Conference on the Physics of Electronic and Atomic Collisions (Abstracts of Papers)* (North-Holland, Amsterdam, 1971), Vol. 1, p. 143.

⁶M. Barat, D. Dhucq, R. François and V. Sidis, *J. Phys. B* **6**, 2072 (1973).

⁷M. Barat, D. Dhucq, R. François, C. Lesech, and R. McCaroll, *J. Phys. B* **6**, 1206 (1973).

⁸F. J. Eriksen, S. M. Fernandez, A. V. Bray, and E. Pollack, *Abstracts of Third International Confer-*

ence on Atomic Physics, Boulder, 1972, p. 70 (unpublished).

⁹R. Morgenstern, M. Barat, and D. C. Lorents, *J. Phys. B* **6**, L330 (1973).

¹⁰M. Barat, J. C. Brenot, and J. Pommier, *J. Phys. B* **6**, L105 (1973); J. C. Brenot, J. Pommier, and M. Barat, *ibid.* (to be published).

¹¹F. T. Smith, *Phys. Rev.* **179**, 111 (1969).

¹²C. C. J. Roothaan, *Rev. Mod. Phys.* **23**, 69 (1951).

¹³R. McCaroll and R. D. Piacentini, *J. Phys. B* **4**, 1026 (1971); M. Barat, D. Dhucq, R. François, R. McCaroll, R. D. Piacentini, and A. Salin, *J. Phys. B* **5**, 1343 (1972).

¹⁴G. Gerber, R. Morgenstern, and A. Nichaus, *J. Phys. B* **6**, 493 (1973).

¹⁵C. Lehmann and G. Liebfried, *Z. Phys.* **172**, 465 (1962); F. T. Smith, R. P. Marchi, and K. G. Dedrick, *Phys. Rev.* **150**, 79 (1966).

¹⁶J. T. Park, V. Pol, J. Lawler, and J. George, *Phys. Rev. Lett.* **30**, 1013 (1973).

¹⁷E. Everhart, G. Stone, and R. J. Carbone, *Phys. Rev.* **99**, 1287 (1955).

¹⁸Q. C. Kessel and B. Fastrup, *Case Studies in Atomic Physics* (North-Holland, Amsterdam, 1973).

¹⁹M. Barat, J. Baudon, M. Abignoli, and J. C. Houver, *J. Phys. B* **3**, 230 (1970).

²⁰D. J. Bierman and W. C. Turkenburg, *Phys. Rev. Lett.* **25**, 633 (1970); D. J. Bierman, W. C. Turkenburg, and C. P. Bhalla, *Physica* **60**, 357 (1972).

²¹V. Sidis and H. Lefebvre-Brion, *J. Phys. B* **4**, 1040 (1971).

²²J. P. Gauyacq, Thèse de 3e Cycle (Université de Paris VI, 1974) (unpublished).

²³P. S. Bagus, B. Liu, A. D. McLean, and M. Yoshimine of the theoretical chemistry group at IBM research in San José, Calif. Preliminary descriptions of the ALCHEMY program are given by McLean [in *Proceedings of the Conference on Potential Energy Surfaces in Chemistry* (California U. P., Santa Cruz, 1970)] and by Bagus [in *Selected Topics in Molecular Physics* (Berlin, 1972)]. See also IBM Research Pub-

- lication No. 14748, 1971 (unpublished).
- ²⁴T. L. Gilbert and A. C. Wahl, *J. Chem. Phys.* **47**, 3425 (1967).
- ²⁵E. W. Thulstrup and H. Johansen, *Phys. Rev. A* **6**, 206 (1972).
- ²⁶R. Daudel, R. Lefebvre and C. Moser, *Quantum Chemistry* (Interscience, New York, 1959), p. 475.
- ²⁷F. T. Smith, R. P. Marchi, W. Aberth, D. C. Lorents, and O. Heinz, *Phys. Rev.* **161**, 31 (1967); J. Baudon, M. Barat, and M. Abignoli, *J. Phys. B* **3**, 207 (1970).
- ²⁸V. Kempter and L. Zehnle (unpublished).
- ²⁹R. C. Amme and P. O. Haugsjaa, *Phys. Rev.* **177**, 230 (1969).
- ³⁰J. Baudon, M. Barat, and M. Abignoli, *J. Phys. B* **3**, 207 (1970).
- ³¹V. Sidis, M. Barat, and D. Dhucq, *J. Phys. B* (to be published).
- ³²A. A. Abrahamson, *Phys. Rev.* **178**, 76 (1969); F. T. Smith, *VII ICPEAC*, edited by T. R. Govers and F. J. DeHeer (North-Holland, Amsterdam, 1972), p. 1; R. G. Gordon and Y. S. Kim, *J. Chem. Phys.* **56**, 3122 (1972); J. C. Bellum and D. A. Micha, *Int. J. Quantum Chem.* (to be published); V. I. Gaydaenko and V. K. Nikulin, *Chem. Phys. Lett.* **7**, 360 (1970).
- ³³P. O. Haugsjaa and R. C. Amme, *Phys. Rev. Lett.* **23**, 633 (1969).
- ³⁴M. C. Hayden and R. C. Amme, *Phys. Rev.* **141**, 30 (1966).
- ³⁵R. François, Thèse de Doctorat d'Etat (Université de Paris XI, 1974) (unpublished).
- ³⁶See for instance D. C. Lorents, W. Aberth, and V. W. Hesterman, *Phys. Rev. Lett.* **17**, 249 (1966); W. Lichten, *Phys. Rev.* **131**, 229 (1963).
- ³⁷R. E. Olson, *Phys. Rev. A* **5**, 2094 (1972); S. A. Evans and N. F. Lane, *ibid.* **8**, 1385 (1973).
- ³⁸M. Barat and W. Lichten, *Phys. Rev. A* **6**, 211 (1972).